Rotordynamic Force Coefficients of a Hybrid Brush Seal: Measurements and Predictions

Luis San Andrés
Mast-Childs Professor
Fellow ASME
e-mail: lsanandres@mengr.tamu.edu

José Baker
e-mail: jose.baker@kbr.com

Adolfo Delgado
e-mail: delgadoa@ge.com

Department of Mechanical Engineering,
Texas A&M University,
College Station, TX 77843

Brush seals effectively control leakage in air breathing engines, albeit only applied for relatively low-pressure differentials. Hybrid brush seals (HBS) are an alternative to resolve poor reliability resulting from bristle tip wear while also allowing for reverse shaft rotation operations. A HBS incorporates pads contacting the shaft on assembly; and which under rotor spinning, lift off due to the generation of a hydrodynamic pressure. The ensuing gas film prevents intermittent contact, reducing wear, and thermal distortions. This paper presents rotordynamic measurements conducted on a test rig for evaluation of HBS technology. Single frequency shaker loads are exerted on a test rotor holding a hybrid brush seal, and measurements of rotor displacements follow for operating conditions with increasing gas supply pressures and two rotor speeds. A frequency domain identification method delivers the test system stiffness and damping coefficients. The HBS stiffness coefficients are not affected by rotor speed though the seal viscous damping shows a strong frequency dependency. The identified HBS direct stiffness decreases ~15% as the supply/discharge pressure increases $P_r = 1.7-2.4$. The HBS cross-coupled stiffnesses are insignificant, at least one order of magnitude smaller than the direct stiffnesses. A structural loss factor (γ) and dry-friction coefficient (μ) represent the energy dissipated in a HBS by the bristle-to-bristle and bristle-to-pad interactions. Predictions of HBS stiffness and damping coefficients correlate well with the test derived parameters. Both model predictions and test results show the dramatic reduction in the seal equivalent viscous damping coefficients as the excitation whirl frequency increases.
[DOI: 10.1115/1.3159377]

1 Introduction

Parasitic secondary flow (seal leakage) in gas turbines represents a considerable loss in power delivery with an increase in specific fuel consumption [1]. Chupp et al. [2] reviewed all types of seals in steam and gas turbines, discussed the different sealing environments in a turbomachinery, and highlighted the benefits resulting from proper clearance control. In a high-pressure turbine, a 0.0254 mm (0.001 in.) blade tip clearance increase renders up to a 0.1% rise in specific fuel consumption and 1°C rise in exhaust gas temperature.

Labyrinth seals are most common in turbomachinery, yet their sealing effectiveness depends on maintaining very tight radial clearances. Operational conditions such as thermal expansion and rotor radial excursions produce teeth wear and enlarge the operating clearance, thus also raising secondary leakage and potential for rotordynamic instability [3,4]. Brush seals, occupying less axial space, are a definite improvement to reduce leakage while better accommodating radial rotor excursions without sealing performance degradation. However, excessive bristle tip wear, rotor surface wear, and localized heat generation are well known drawbacks [2,5]. Additionally, conventional brush seals withstand relatively low-pressure differentials and, due to the angled orientation of the bristles, only allow for unidirectional shaft rotation (see Fig. 1). Recently, shoed-brush seals (SBSs) and hybrid brush seals (HBSs) offer a better leakage control with improved reliability while allowing for bidirectional rotation [6–8]. In addition, due to their low radial stiffness, HBS can better accommodate rotor radial excursions without affecting their sealing capability. Under certain circumstances, a HBS may also act as an effective vibration damper [7].

The following review focuses on the rotordynamic forced performance characteristics of labyrinth and brush seals. The magisterial paper of Chupp et al. [2] reviews the literature related to the leakage performance, experimental and analytical, of these types of seals. Benckert and Wachter [9] first discussed the effect of pressure differential, rotor speed, inlet flow conditions, and seal geometry on the rotordynamic stability of labyrinth seals. Tests results show that the inlet swirl velocity of a gas entering a labyrinth seal or developed within its cavities (due to shaft rotation) generates destabilizing forces (i.e., cross-coupled stiffness), therefore reducing the effective damping of the seal. As a corrective measure, "swirl brakes" are implemented upstream of the labyrinth seal to reduce and, in some cases, even eliminate the preswirl entering a seal. References [3,4] present the analysis for prediction of fluid film forces in labyrinth seals and discussed the extensive experimental data related to rotordynamic force coefficients, with emphasis on their influence on the stability of rotor-bearing systems.

Initially implemented in aerospace applications, brush seals are presently an essential component in power generation turbomachinery, offering significant efficiency improvement and reducing fuel consumption [10]. Commercial brush seals consist of packed metallic (or polymer) bristles of fine diameter, clamped between a front plate on the upstream (high-pressure region), and a backing plate on the downstream (low pressure region), as shown in Fig. 1. Bristles are slanted at an angle (i.e., lay angle) in the direction of rotor spinning. The bristles bend rather than buckle during transient rotor radial excursions.

Conner and Childs [11] presented measurements of rotordynamic coefficients for a four-stage brush seal operating at increasing pressure ratios, shaft speed, fluid prerotation, and seal spacing. Test derived cross-coupled stiffnesses (i.e., source of destabilizing

Contributed by the International Gas Turbine Institute of ASME for publication in the JOURNAL OF ENGINEERING FOR GAS TURBINES AND POWER. Manuscript received March 23, 2009; final manuscript received March 29, 2009; published online January 26, 2010. Review conducted by Dilip R. Ballal. Paper presented at the ASME Gas Turbine Technical Congress and Exposition, Orlando, FL, June 8–12, 2009.

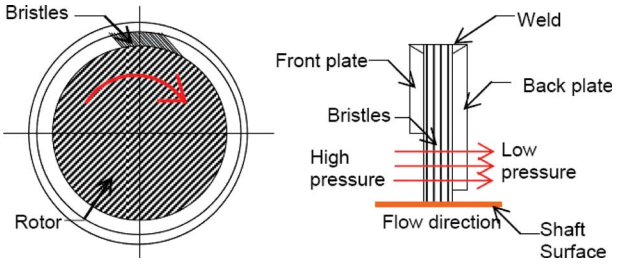

Fig. 1 Axial and cross-sectional views of a conventional brush seal

Fig. 2 Photograph of a hybrid brush seal (close up of pad and elastic supports)

forces in labyrinth gas seals) are very low and generally negative, thus having a stabilizing effect opposite to that in labyrinth seals. Direct damping coefficients increase marginally as a function of rotor speed. The test results demonstrate the apparent rotordynamic benefits of implementing brush seals instead of labyrinth seals in turbomachinery.

Most brush seals work effectively with low-pressure differentials. A high-pressure drop across the seal deflects its bristles in the flow direction and occasionally radially inward (i.e., blowdown effect) due to the low axial stiffness of the bristle matrix. As a result, at times, brush seals are installed or retrofitted in parallel with labyrinth seals. Basu et al. [12] identified pressure induced bristle "hysteresis" and "stiffening" as two major drawbacks of brush seals. Bristle hysteresis prevents displaced bristles from returning to their original position after a rotor radial excursion, increasing the seal leakage since the flow area increases. Furthermore, conventional brush seals are prone to persistent wear due to intermittent contact between the bristles and rotor surface, inducing on most occasions severe local thermal distortions.

Justak and co-worker [6–8] first introduced the multiple SBS and later the HBS to resolve the poor reliability noted above while allowing for bidirectional shaft rotation. Prior to operation, the shoes are in contact and pressing against the rotor surface. With a pressure differential, the pad design allows for a hydrostatic lift-off effect prior to shaft rotation. As the shaft rotates, the hydrostatic pad lift-off is further enhanced by the generation of a hydrodynamic gas film pressure that reduces or eliminates wear during steady operation. San Andrés and co-workers [13,14] reported measurements of leakage, static (nonrotating) structural stiffness of a large diameter shoe brush seal, and developed an accurate and simple predictive model based on thin beam elastic deformation formulas. Impact load tests to identify the dynamic seal, dynamic stiffness, and damping coefficients evidence a nonlinear behavior, making the viscous damping model not suitable for damping response predictions. Hysteresis and dry-friction in the bristle bed characterize the seal mechanical energy dissipation.

Delgado et al. [15] introduced a gas thin film flow analysis for the prediction of rotordynamic force coefficients of SBSs. The physical model couples the gas film forces generated in the thin gap between the rotor and a shoe (pad) and the structural characteristics (stiffness and damping) from the bristle pack underneath. Predictions indicate that rotordynamic force coefficients are independent of the operating gas film clearance and pressure differential across the seal. Predicted direct seal stiffnesses at null rotor speed correlate well with the structural stiffness in Ref. [13] and decrease rapidly with increasing rotor speed. Seal cross-coupled stiffnesses are at least one order of magnitude smaller than the direct stiffnesses. Hysteretic (structural) damping, expressed in terms of a structural loss factor, accounts for most of the seal damping.

Delgado and San Andrés [16] detailed a sound identification method to extract the structural stiffness and damping coefficients of a SBS, 153 mm in diameter, using single frequency dynamic loads in a controlled motion test rig (without shaft rotation) and no gas pressurization. The brush seal energy dissipation mechanism is modeled as a combination of structural damping and Coulomb damping mechanisms, and represented by a loss factor (γ) and a dry-friction coefficient (μ), respectively. The parameter identification method is valid only above a threshold load (i.e., macroslip motion regime), where seal deflections are dependent on the applied load, and the friction force is nearly constant in amplitude. Seal motions below this load evidence the presence of superharmonic frequency component (three and five times) characteristics of systems with dry-friction, and arise from bristle-to-bristle and bristle-to-back plate interaction.

HBSs are an enhancement of the original SBS [8]. As shown in Fig. 2, arcuate pads are connected to the seal casing through electrical discharge machining (EDM) slender spring lever elements. The novel construction eliminates reliability issues associated to the original used spot-welded connections. The thin EDM spring lever connections have a low radial stiffness and high axial stiffness; thus eliminating bristle and rotor wear, and at the same time, preventing pad pitching motions caused by high-pressure differentials across the seal. The bristle matrix is now a secondary seal to the gas film riding pad element.

San Andrés et al. [17] reported the measurements of power loss and leakage in a HBS for increasing pressure differentials and over a range of rotor speeds. Power loss and drag torque measured at low rotor speeds (<11 m/s at 1300 rpm) decrease as the pressure differential across the seal increases. Maximum power losses occur without air pressurization (rubbing between pads and rotor). Power losses decrease by approximately 90% over the test speed range (400–1300 rpm) as the seal is pressurized, evidencing the generation of a hydrodynamic gas film, separating the seal pads from the rotor surface. A low constant temperature ($\sim 25\,^{\circ}$C) at the rotor/seal interface during rotating tests confirms the presence of a gas film, thus eliminating rotor and seal wear. Additionally, leakage measurements at room temperature show an improved sealing ability with a leakage reduction of about 36% when compared with a first generation SBS in Ref. [14].

This paper describes a test rig for measurements of leakage and rotor motions in a HBS, along with the identification of the seal rotordynamic force coefficients. References [17,19] report the measurements of seal leakage and power loss and the identification of static structural stiffness, respectively.

2 Description of Test Rig and HBS

Figure 3 depicts the HBS rotordynamic test rig and its instrumentation. A slender steel shaft is affixed to the base of a cylindrical steel vessel via two tapered roller bearings. The free end of the shaft holds a steel disk where the test seal is located.

Two eddy current sensors, 90 deg apart, are secured on the front plate of the vessel and face the outer diameter of the steel disk, as shown in Fig. 4. The sensors record the disk displacements along two orthogonal directions in the vertical plane. A slender rod (stinger) with load cell connects an electromagnetic shaker to the free end of the shaft. Two soft springs located at the drive end of the shaft, in the vertical and horizontal directions, allow the centering of the rotor free end with respect to the test seal. The springs connect to the shaft through a ball bearing. At the shaft's free end, a small dc motor drives the overhang shaft and disk

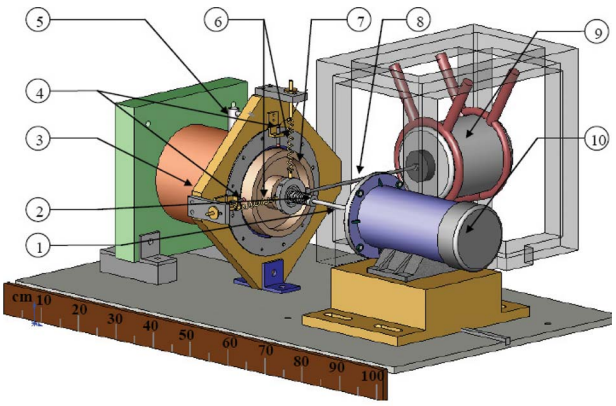

1	Quill shaft	6	Soft centering springs
2	Flexible coupling	7	Rotor
3	Pressurization vessel	8	Stinger
4	Eddy current sensors	9	Electromagnetic shaker
5	Supply pressure inlet	10	DC motor

Fig. 3 Isometric view of rotordynamic test rig for evaluation of hybrid brush seal

assembly through a flexible coupling. A pressurized air line, feeding into the cylindrical vessel, is instrumented with multiple pressure taps, a turbine flow meter, a static pressure transducer, and thermocouples. Presently, all measurements are conducted at room temperature (25°C).

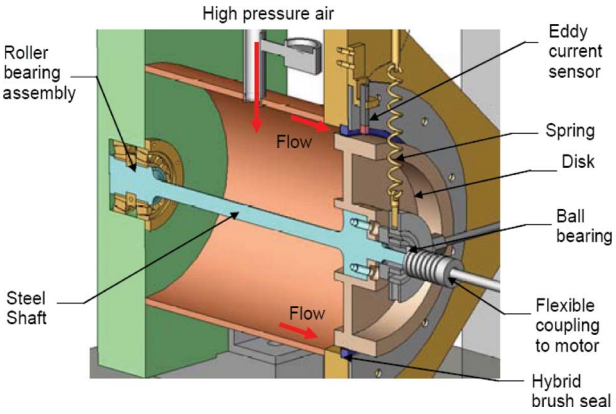

Fig. 4 Detail view of disk/shaft assembly

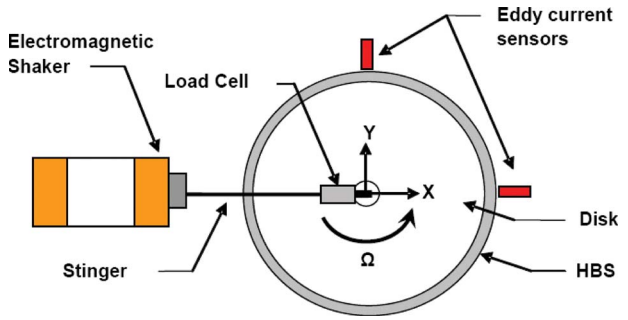

Fig. 5 Reference coordinate system for rotating tests with shaker loads

Table 1 details the test seal dimensions, material properties, and operating conditions for measurements of seal leakage and force coefficients. Baker [18] detailed the measurement of the disk and shaft's system natural frequencies and vibration mode shapes and reported the system equivalent stiffness and mass coefficients. Reference [19] presents single frequency dynamic load tests (without shaft rotation) to identify the seal equivalent viscous damping coefficient. Mechanical energy dissipation parameters are identified for increasing supply pressures. The dry-friction coefficient (μ) increases slightly as the test pressure ratio[1] increases (5% from P_r=1.0 to P_r=3). The increase in the dry-friction coefficient is directly related to the increase in the contact forces between the seal components induced by the pressure differential across the seal. The loss factor coefficient (γ) (material hysteresis) decays as the pressure ratio increases. This behavior is attributed to the repositioning of the bristles and the stiffening effect due to the pressure differential across the seal (i.e., blowdown effect).

3 Measurements and Parameter Identification Method

Presently, in the rotordynamic measurements with a centered seal, the gas supply pressure (P_s) is manually adjusted (169 kPa and 238 kPa), and the motor is turned on to bring the test rotor to a constant speed (600 rpm and 1200 rpm). As the shaft spins, the electromagnetic shaker excites the test seal with a periodic load, amplitude of 22 N,[2] and single frequency ranging from 20 Hz to 80 Hz (3 Hz increments). Figure 5 shows the reference coordinate

[1]Pressure ratio $P_r=P_s/P_d$=absolute supply pressure/absolute discharge pressure.

[2]Smaller load magnitudes lead to stick-slip (nonlinear) phenomenon with erratic seal behavior, while larger magnitude loads produce too large rotor displacements that endanger the seal life.

Table 1 Dimensions and material properties of test hybrid brush seal

Physical Properties	SI Unit	U.S. unit
Rotor diameter, D_j	167.1 mm	6.580 in.
Brush seal (pads) inner diameter, Ds_i	166.4 mm	6.550 in.
Brush seal (retainer) outer diameter, D_o	183.1 mm	7.210 in.
Brush seal width, B_w	8.53 mm	0.336 in.
Radial interference between rotor and seal, R_i	0.381 mm	0.015 in.
Number of pads	20	
Width of pads	7.23 mm	0.331 in.
Bristle lay angle, α	45 deg	-
Bristle modulus of elasticity, E	22.48×10^5 bars	32.6×10^6 psi
Bristle density (circumference)	850 bristles/cm	2300 bristles/in.
Fluid: air	SI unit	U.S. unit
Pressure downstream (discharge), P_d	101 kPa	14.54 psi (absolute)
Pressure upstream (supply), P_s	136–307 kPa	19.7–44.5 psi (absolute)
Temperature upstream, T_u	69–71°F	20.5–21.7°C
Rotor speed, Ω	0 rpm, 600 rpm, and 1200 rpm	

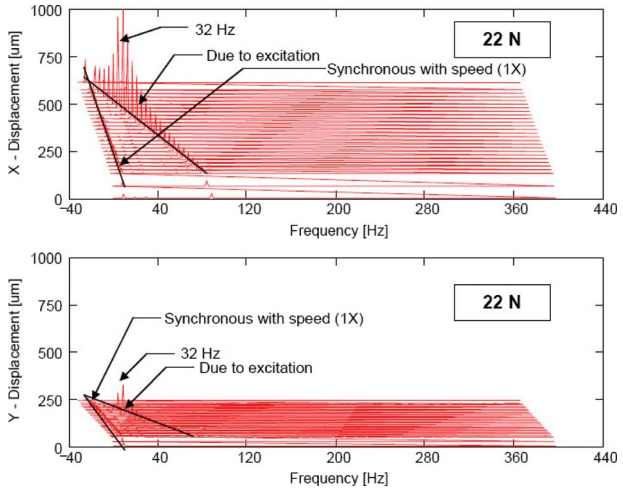

Fig. 6 Waterfalls of rotor displacements (*X*, *Y*) resulting from a periodic excitation load (22 N). Excitation frequency range of 20–90 Hz, P_r=1.7, and rotor speed: 600 rpm (10 Hz).

system used for the rotordynamic tests. The *X*-direction is collinear with the periodic excitation load.

Figure 6 depicts the waterfall plot for the disk's forced motions along the *X*- and *Y*-directions. The response amplitudes *X* due to the applied load excitation increases as it approaches the test system's natural frequency, i.e., ~32 Hz. The disk motion in the *Y*-direction is much smaller (i.e., at least one order of magnitude) than that in the *X*-direction, thus indicating a minimal cross-coupling effect. Similar behavior is shown at 1200 rpm and 238 kPa absolute supply pressure. Hence, the measurements evidence little cross-coupling effects of the test seal. Furthermore, note that the effect of remnant rotor imbalance on the recorded motions (one time) is minimal. Hence, disk motions at this frequency can be easily filtered from the others induced by the dynamic load excitation.

Incidentally, Baker [18] modeled the test rotor and HBS system and predicted, as a function of rotor speed, the first forward and backward natural frequencies, see Table 2. The analysis and experimental verification show that gyroscopic (rotor stiffening) effects affect minimally the rotor system response for the low shaft speeds (Ω) considered.

The observations above permit reducing the degrees of freedom of the test system, and enable the implementation of a simple model to identify the rotordynamic coefficients of the HBS, as detailed in Ref. [15]. In brief, the equations of motion for the equivalent mechanical system representing the test rotor and HBS are

$$\begin{bmatrix} M_{xx} & M_{xy} \\ M_{yx} & M_{yy} \end{bmatrix} \begin{Bmatrix} \ddot{x} \\ \ddot{y} \end{Bmatrix} + \begin{bmatrix} K_{xx} & K_{xy} \\ K_{yx} & K_{yy} \end{bmatrix} \begin{Bmatrix} x \\ y \end{Bmatrix} + \begin{bmatrix} C_{xx} & C_{xy} \\ C_{yx} & C_{yy} \end{bmatrix} \begin{Bmatrix} \dot{x} \\ \dot{y} \end{Bmatrix} = \begin{pmatrix} F_x \\ 0 \end{pmatrix} + \begin{pmatrix} F_{ix} \\ F_{iy} \end{pmatrix} \tag{1}$$

where $\{M_{\alpha\beta}, \quad K_{\alpha\beta}, \quad \text{and} \quad C_{\alpha\beta}\}_{\alpha\beta=x,y}$ are the *test system*[3] mass, stiffness, and equivalent *viscous* damping coefficients, respectively. F_x is the excitation force (loading in the *X*-direction only) with frequency ω, i.e., $F_x=\bar{F}e^{i\omega t}$. F_{ix} and F_{iy} are the *imbalance* forces with a frequency coincident with shaft speed Ω. The test system displacements due to the periodic force are $x=\bar{x}e^{i\omega t}$ and $y=\bar{y}e^{i\omega t}$. Hence, Eq. (1) reduces to

$$Z_{xx}\cdot\bar{x} + Z_{xy}\cdot\bar{y} = \bar{F}_x \tag{2a}$$

$$Z_{yx}\cdot\bar{x} + Z_{yy}\cdot\bar{y} = 0 \tag{2b}$$

where $Z_{\alpha\beta}=\{K_{\alpha\beta}-M_{\alpha\beta}\omega^2+iC_{\alpha\beta}\omega\}_{,\alpha\beta=x,y}$ represent the test system impedances. For small rotor displacements about a seal centered position, one reasonably asserts that $Z_{xx}=Z_{yy}$ and $Z_{xy}=-Z_{yx}$. Hence, the direct and cross-coupling impedances are readily identified using the amplitude and phase information at the frequency of interest ($\omega\neq\Omega$),

$$Z_{xx}=Z_{yy}=\frac{\bar{F}_x\cdot\bar{x}}{(\bar{x}^2+\bar{y}^2)} \quad \text{and} \quad Z_{yx}=-Z_{xy}=-Z_{yy}\frac{\bar{y}}{\bar{x}} \tag{3}$$

Table 2 Predicted natural frequencies (forward and backward) for test rotor with HBS in place (Ref. [18])

Rotor speed (rpm)	Natural frequency (Hz) First predicted	Measured P_r=1.7	Measured P_r=2.4	Second model
0	30.5	34.0	38.5	146
600	29.7/31.4	32.5	36.6	154
1200	28.8/32.2	31.1	36.3	163
	Backward/forward			Away from test frequency range

[3]Refer to Ref. [16] or [19] for details on the physical model relying on equivalent stiffness and mass parameters representing the combined actions of the shaft+disk+seal, and derived from mechanical energy considerations for motions exciting the fundamental elastic mode.

Table 3 Identified test system direct stiffness and mass coefficients, and HBS stiffness. Load 22 N, 20–80 Hz, increasing pressure ratios (P_r).

	Tests with rotor spinning			
Pressure ratio	P_r=1.7		P_r=2.4	
Rotor speed, Ω (rpm)	600	1200	600	1200
Stiffness, K_{xx} (kN/m)	108(±6)	98(±5)	130(±6)	124(±6)
Mass, M_{xx} (kg)	2.62	2.54	2.43	2.39
R^2 (correlation factor) dynamic stiffness ($K_{xx}-M_{xx}\omega^2$)	0.98	0.98	0.98	0.98
HBS stiffness, K_s (kN/m)	103(±5)	89(±4)	135(±6)	128(±6)
HBS dry-friction coefficient, μ	0.39	0.36	0.37	0.38
HBS loss factor coefficient, γ	0.29	0.26	0.33	0.34
	Nonrotating tests			
Pressure ratio	P_r=1.0	P_r=1.7	P_r=2.4	P_r=3.0
HBS stiffness (kN/m)	93(±5)	130(±6)	141(±7)	141(±7)
Dry-friction coefficient, μ	0.66	0.51	0.64	0.69
Loss factor coefficient, γ	0.42	0.40	0.27	0.22

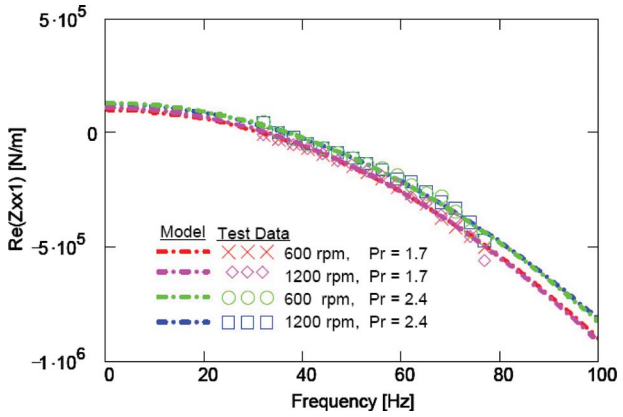

Fig. 7 Identified system rotordynamic stiffness versus frequency. Load magnitude=22 N for increasing supply pressure to discharge pressure ratios (P_r) and rotor speeds.

4 Identified HBS Rotordynamic Force Coefficients

Table 3 presents the test system direct stiffness (K_{xx}), mass coefficient (M_{xx}), and the derived HBS stiffness (K_s) for increasing supply pressures and rotor speeds. The system stiffness ($K_{xx}=K_{yy}$) and the HBS stiffness (K_s) decrease ~15% as the rotor speed increases from 600 rpm to 1200 rpm for $P_r=1.7$ and 5% for $P_r=2.4$. The table includes the identified dry-friction (μ) and loss factor (γ) coefficients representing the mechanical energy dissipation of the seal. These coefficients show little variation with rotor speed for the test pressure ratios $P_r=1.7$ and 2.4. The seal stiffness coefficient identified from the tests with shaft rotation (600 rpm and 1200 rpm) shows a similar increasing trend with the pressure ratio as the seal stiffness from tests without shaft rotation.

Figure 7 depicts the real part of the test system impedance $\mathrm{Re}(Z_{xx})=(K_{xx}-M_{xx}\omega^2)$ obtained from rotordynamic tests for a load of 22 N. The figure illustrates the good correlation between test data (force and displacement) and the curve fit generated by the identified force coefficients in Table 3.

Figure 8 shows the HBS equivalent viscous damping coefficient (C_{eq}) derived from the test data and physical model predictions that integrate the dry-friction (μ) and structural damping (γ) parameters in Table 3. The viscous damping coefficient drops dramatically with the excitation frequency toward a minimum at the test system's natural frequency (~32 Hz). The equivalent damping coefficients are typical for a structure with dry-friction damping, i.e., motion amplitude and frequency dependent, $C_{eq}\sim 1/\bar{x}\omega$.

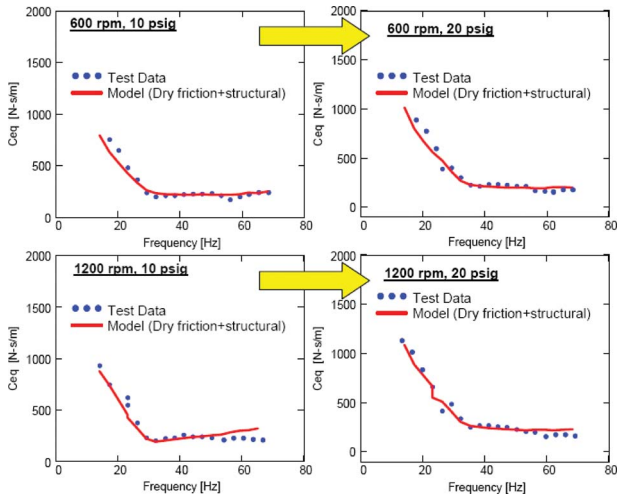

Fig. 8 Test data and identified HBS equivalent viscous damping for increasing rotor speeds (600 rpm and 1200 rpm) and two pressure ratios (P_r=1.7 and 2.4)

Table 4 Identified test system cross-coupled force coefficients from rotordynamic tests. Load 22 N, 20–80 Hz, for increasing pressure ratios (P_r).

Pressure ratio	P_r=1.7		P_r=2.4	
Rotor speed, Ω (rpm)	600	1200	600	1200
Stiffness, K_{xy} (kN/m)	8.8	15	2.7	6.6
Mass, M_{xy} (kg)	0	0	0	0

Table 4 shows the identified cross-coupled force coefficients ($K_{xy}=-K_{yx}$) from the rotordynamic tests at increasing supply pressures. Results indicate that the cross-coupled masses are nearly 0 kg and in some instances slightly negative, thus indicating that the equivalent cross-coupled dynamic stiffness is independent of the excitation frequency. In addition, identified cross-coupled stiffness values are considerably smaller (up to one order of magnitude) than the identified direct coefficients.

5 Predictions of HBS Rotordynamic Force Coefficients

Frequency dependent rotordynamic force coefficients for the test HBS are obtained using the thin film gas flow-structure model in Ref. [15]. In a centered seal, there is rotational symmetry, and hence, the direct force coefficients are identical, and cross-coupled coefficients are antisymmetric, e.g., $K_{sxx}=K_{syy}$ and $K_{sxy}=-K_{syx}$. Figure 9 shows the predicted HBS stiffness coefficients (K_{sxx}) versus the excitation frequency (20–100 Hz) at a rotor speed of 600 rpm and 1200 rpm, and two supply to discharge pressure ratios $P_r=1.7$ and 2.4. Predictions indicate that increasing the pressure ratio $P_r=P_s/P_d$ has a negligible effect on the HBS direct stiffness K_{sxx}. The direct seal stiffness shows a small dependency on the excitation frequency. The predicted cross-coupled stiffness (K_{sxy}) is at least one order of magnitudes less than the direct stiffness, thus, not shown for clarity. For reference, the dashed lines denote the HBS seal stiffness (frequency independent) identified from the rotordynamic test results at $P_r=1.7$. The direct HBS stiffness K_{sxx} drops at approximately 10% as the rotor speed increases to 1200 rpm while showing no dependence on the excitation frequency. The test results validate the code predictions.

Figure 10 shows the predicted HBS viscous damping coefficients ($C_{sxx}=C_{syy}$) versus the excitation frequency and for constant rotor speeds, 600 rpm and 1200 rpm, and two pressure ratios,

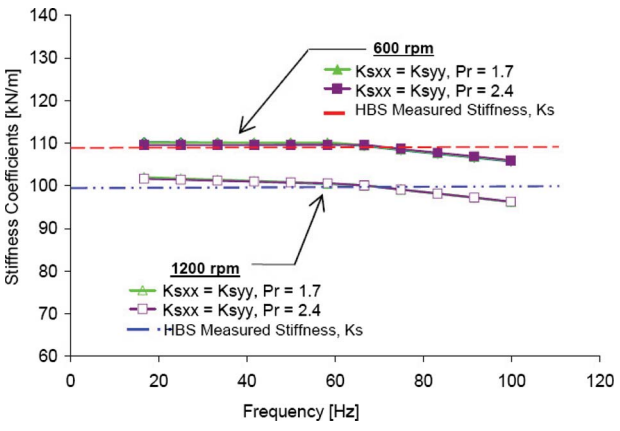

Fig. 9 Predicted nonsynchronous HBS stiffness coefficients versus excitation frequency at two supply to discharge pressure ratios, P_r=1.7 and 2.4. Rotor speeds: 600 rpm (10 Hz) and 1200 rpm (20 Hz).

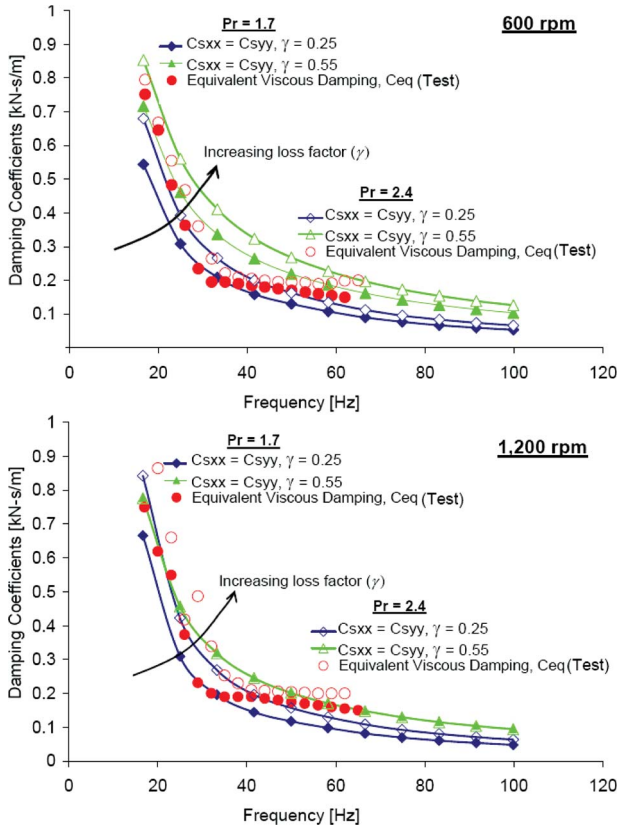

Fig. 10 Predicted HBS viscous damping coefficients versus excitation frequency. Rotor speeds: 600 rpm (10 Hz) and 1200 rpm (20 Hz); supply to discharge pressure ratio, P_r=1.7 and 2.4.

P_r=1.7 and 2.4. Predictions show the HBS damping C_{sxx} decays rapidly with increasing excitation frequency (ω). C_{sxx} increases as a function of increasing structural loss factor coefficient (γ), which accounts for the hysteretic effect of the bristle bed. The figure also includes the HBS equivalent viscous damping ($C_{eq} \sim C_{sxx}$) derived using the test data obtained from the rotordynamic experiments. The loss factor (γ) and dry-friction (μ) identified from C_{eq} range between 0.20–0.45 and 0.35–0.69, respectively. The predicted HBS damping C_{sxx} at 600 rpm and 1200 rpm are nearly identical with minimal dependence on the test seal pressure ratio.

The largest uncertainties of the identified dry-friction (μ) and structural loss factor (γ) are 8% and ~12%, respectively. The uncertainty estimation follows the procedure described in Refs. [18–20] that accounts for the instrument's precision error, the error associated with the curve fit, and the repeatability of the tests.

6 Conclusions

HBSs offer advantages when compared with labyrinth seals in terms of leakage, power loss, and dynamic forced performance. In addition, a HBS overcomes the main deficiencies of conventional brush seals such as excessive rotor and seal wear due to sustained contact between these two components, low-pressure differential sealing capacity, and unidirectional rotation.

Further progress on the evaluation of reliability of HBS technology for applications in gas turbine engines is reported. This paper details a test rig for measurement of leakage, power loss, and rotordynamic coefficients of shoed-brush seals. References [16–18] report measurements of leakage and power loss for increasing pressure differentials and rotor speeds. Presently, experiments are conducted to identify the HBS rotordynamic force coefficients from unidirectional single frequency forcing functions while the seals operate under pressurized conditions and with rotor spinning. A frequency domain parameter identification model extracts the seal force coefficients from the measured displacements/force transfer functions.

The test system direct stiffness coefficients (K_{xx}) decrease at about 15% and 5% with increasing rotor speed of 600–1200 rpm for supply to discharge pressure ratios P_r=1.7 and 2.4, respectively. The predicted seal stiffness (K_{sxx}) for 600 rpm and 1200 rpm correlates well (less than 5%) with the seal stiffness (K_s) identified from rotordynamic tests at increasing pressure ratios. The seal cross-coupled stiffness ($K_{sxy}=-K_{syx}$) is at least one order of magnitude smaller than the seal direct stiffness (K_{sxx}). The seal predicted direct damping coefficients (C_{sxx}) are approximately equal to the equivalent viscous damping ($C_{eq} \sim C_{sxx}$) derived from the test data for γ=0.25–0.55. The seal viscous damping coefficient (C_{sxx}) diminishes as a function of increasing excitation frequency, reaching a minimum value at the natural frequency of the test system (~32 Hz) with marginal dependence on rotor speed or supply pressure.

Incorporating a HBS in turbomachinery will reduce leakage and power losses with savings in fuel consumption, operation and maintenance costs, and increased engine reliability. Further testing of the seal at higher gas temperatures and higher rotor speeds is underway to replicate the actual operating environment of an engine.

Acknowledgment

The continued support of Siemens Power Generation is gratefully acknowledged. Thanks to Advanced Technologies Group (www.advancedtg.com) for donating the test hybrid brush seal.

Nomenclature

C_{eq} = hybrid brush seal equivalent viscous damping coefficient (Ns m)
$C_{\alpha\beta}$ = test system viscous damping coefficient (Ns m); α, β: x, y
$C_{s\alpha\beta}$ = predicted seal viscous damping coefficient (Ns m); α, β: x, y
$F_{ix,iy}$ = imbalance force along X- and Y-directions (N)
F_x = excitation force along the X-direction (N)
K_{ij} = equivalent stiffness for test system (N/m); α, β: x, y
K_{sij} = predicted seal stiffness coefficients (N/m); α, β: x, y
K_s = hybrid brush seal stiffness (N/m)
$M_{\alpha\beta}$ = test system mass (kg); α, β: x, y
P_d = absolute discharge pressure (Pa)
P_s = absolute supply pressure (Pa)
P_r = pressure ratio (P_s/P_d)
x, y = shaft displacement along X- and Y-directions (m)
t = time (s)
α = bristle lay angle (deg)
γ = loss factor coefficient
μ = brush seal dry-friction coefficient
Ω = rotor speed (rpm)
ω = excitation frequency (rad/s)

Complex Variables in Frequency Domain

$\bar{F}$ = complex amplitude of force (N)
$\bar{x}, \bar{y}$ = complex amplitude of displacement (m)
$Z_{\alpha\beta}$ = frequency domain impedance function (N/m); α, β: x, y

References

[1] Proctor, M. E., and Delgado, I. R., 2004, "Leakage and Power Loss Tests

Results for Competing Turbine Engine Seals," NASA Report No. TM-2004-213049.
[2] Chupp, R. E., Hendricks, R. C., Lattime, S. B., and Steinetz, B. M., 2006, "Sealing in Turbomachinery," J. Propul. Power, **22**(2), pp. 313–349.
[3] Childs, D., 1993, *Turbomachinery Rotordynamics*, Wiley, New York, Chap. 5.
[4] Childs, D., and Vance, J. M., 1997, "Annular Gas Seals and Rotordynamics of Compressors and Turbines," *Proceedings of the 26th Turbomachinery Symposium*, Houston, TX, pp. 201–220.
[5] Dogu, Y., and Aksit, M. F., 2006, "Brush Seal Temperature Distribution Analysis," ASME J. Eng. Gas Turbines Power, **128**(3), pp. 599–609.
[6] Justak, J. F., 2002, "Robust Hydrodynamic Brush Seal," U.S. Patent No. 6,428,009.
[7] Justak, J. F., and Crudgington, P. F., 2006, "Evaluation of a Film Riding Hybrid Seal," AIAA Paper No. 2006-4932.
[8] Justak, J. F., 2007, "Hydrodynamic Brush Seal," U.S. Patent No. 7,182,345.
[9] Benckert, H., and Wachter, J., 1980, "Flow Induced Spring Coefficients of Labyrinth Seals for Applications in Turbomachinery," NASA Report No. CP2133.
[10] Chupp, R. E., and Dowler, C. A., 1993, "Performance Characteristics of Brush Seals for Limited-Life Engines," ASME J. Eng. Gas Turbines Power, **115**, pp. 390–396.
[11] Conner, J. K., and Childs, D., 1993, "Rotordynamic Coefficient Test Results for a Four-Stage Brush Seal," J. Propul. Power, **9**(3), pp. 462–465.
[12] Basu, P., Datta, A., Loewenthal, R., and Short, J., 1994, "Hysteresis and Bristle Stiffening Effects in Brush Seal," J. Propul. Power, **10**(4), pp. 569–575.
[13] Delgado, A., San Andrés, L., and Justak, J., 2003, "Identification of Stiffness and Damping Coefficients in a Shoed Brush Seal," *Proceedings of the Seventh Congreso y Exposicion de Latinoamericana Turbomaquinaria*, Veracruz, Mexico, pp. 1–7.
[14] Delgado, A., and San Andrés, L., 2005, "Measurements of Leakage, Structural Stiffness and Energy Dissipation Parameters in a Shoed Brush Seal," Sealing Technol., **2005**(12), pp. 7–10.
[15] Delgado A., San Andrés L., and Justak J. F., 2004, "Analysis of Performance and Rotordynamic Force Coefficients of Brush Seals With Reverse Rotation Ability," ASME Paper No. GT2004-53614.
[16] Delgado, A., and San Andrés, L., 2007, "Identification of Structural Stiffness and Damping Coefficients of a Shoed-Brush Seal," ASME J. Vibr. Acoust., **129**(5), pp. 648–655.
[17] San Andrés, L., Baker, J., and Delgado, A., 2009, "Measurements of Leakage and Power Loss in a Hybrid Brush Seal," ASME J. Eng. Gas Turbines Power, **131**(1), p. 012505.
[18] Baker, J., 2007, "Measurements of Leakage, Power Loss and Rotordynamic Force Coefficients in a Hybrid Brush Seal," MS thesis, Texas A&M University, College Station, TX.
[19] San Andrés, L., Baker, J., and Delgado, A., 2008, "Measurement of Leakage and Identification of Structural Force Coefficients in a Hybrid Brush Seal," *Proceedings of the STLE Annual Meeting and Exhibition*, Cleveland, OH, pp. 19–21.
[20] Coleman, H. W., and Steele, G. W., 1988, *Experimentation and Uncertainty Analysis for Engineers*, Wiley, New York, Chaps. 1–4.